IJBBE International Journal of Biophotonics & Biomedical Engineering Vol. 4, No. 1, Spring-Summer, 2024

Research Article

Optical Properties of Coupled Gold Nanoparticles: A Numerical Study for Photothermal Applications

V. Rajabpour [1] and R. Rasooli Saghai [1, *]

1 Faculty of Electrical and Computer Engineering, University of Tabriz, Tabriz, Iran

***Corresponding author: raharasouli98@gmail.com**

DOI: 10.71498/ijbbe/2024.1129191

ABSTRACT

Received: Aug. 15, 2024, Revised: Jan. 1, 2025, Accepted: Jan. 2, 2025, Available Online: Jan. 29, 2025

Photothermal therapy (PTT) using plasmonic nanoparticles, particularly gold, is a promising method for cancer cell ablation. However, optimizing the morphology and size of nanoparticles for efficient light absorption and heat conversion remains challenging. Plasmonic metamolecules, like gold nanodimers, demonstrate significant localized field enhancement and strong infrared light absorption. In this study, we investigate gold nanoparticles with spherical, rod, pyramid, and cubic morphologies in both monomeric and dimeric forms. For dimer structures, side-by-side and end-to-end couplings were considered. Our analysis includes parameters such as absorption cross-section, photothermal conversion efficiency (PCE), and field enhancement to compare the optical properties of these nanostructures within the first biological window. Our findings suggest that gold nanopyramids, with their suitable PCE, intermediate peak wavelength spacing in side-by-side and end-to-end dimers, and significant local field enhancement, are more controllable candidates for photothermal applications.

KEYWORDS

Photothermal Therapy, Localized Surface Plasmon Resonance, Gold Nanodimers, Nanorod, Nanopyramid, Nanocube, Field Enhancement.

I. INTRODUCTION

Photothermal therapy (PTT) has emerged as a promising minimally invasive technique for cancer treatment, leveraging the conversion of light energy into heat to ablate tumor cells [1, 2]. This method offers several advantages, including precise targeting and minimal damage to surrounding healthy tissues [3]. The unique properties of nanoparticles, particularly gold nanoparticles (AuNPs), have made them ideal candidates for enhancing the efficacy of PTT [4]. One of the key phenomena that underpin the effectiveness of AuNPs in PTT is localized surface plasmon resonance (LSPR), which occurs when conduction electrons on the nanoparticle surface oscillate in resonance with incident light [5]. The LSPR effect in metallic nanoparticles, such as gold, is highly sensitive to several parameters, including particle size,

shape, and the dielectric environment [6]. These parameters significantly influence the absorption and scattering properties of the nanoparticles, thereby affecting their photothermal conversion efficiency (PCE) [7].

In the context of biomedical applications, the concept of biological windows is crucial [6]. These windows refer to specific wavelength ranges (typically in the near-infrared region) where biological tissues exhibit minimal absorption and scattering, allowing deeper light penetration [8]. This characteristic is essential for effective PTT, as it ensures that the therapeutic light can reach deeper-seated tumors [9]. The coupling of gold nanoparticles can further modify their optical properties, leading to enhanced LSPR effects and improved photothermal performance [10]. Coupled nanoparticles exhibit collective oscillations that can result in stronger electromagnetic fields and increased heat generation [11]. This phenomenon is particularly beneficial for PTT, as it can lead to more efficient tumor ablation with lower light doses.

Understanding the impact of nanoparticle coupling on their optical behavior is essential for optimizing their design for PTT applications [12]. The arrangement and distance between coupled nanoparticles can significantly influence their LSPR response, thereby affecting their overall photothermal efficiency [13]. Researchers have been investigating various configurations and materials to maximize the therapeutic potential of these nanoparticles. Several studies have explored the simulation and experimental validation of coupled gold nanoparticles to elucidate their enhanced optical properties. For instance, In [14], the authors demonstrated the superior photothermal efficiency of coupled AuNPs compared to isolated particles. In another work, Sahu et al. [12] highlighted the role of interparticle distance and arrangement in tuning the LSPR response of coupled nanoparticles. Several other studies have also investigated the optical behavior of coupled gold nanoparticles in the form of dimers and trimers [11, 15-18]. These studies underscore the potential of coupled gold nanoparticles in advancing photothermal therapy and other biomedical applications.

In this study, the optical behavior of gold nanoparticles in both monomer and dimer forms was investigated using the finite element method. Initially, the optical properties of monomeric gold nanoparticles with spherical, rod, cubic, and pyramidal morphologies, all having the same volume, were examined. The dimer structures were then formed such that the total volume of the two nanoparticles in the dimer was equal to that of the corresponding monomer. Subsequently, the optical behavior of these gold nanoparticle dimers was studied. Maintaining the same volume for both monomers and dimers helps in assessing the effect of nanoparticle concentration in photothermal applications. Additionally, examining various morphologies, which have not been extensively studied in previous research, can provide valuable insights into the field enhancement capabilities of these nanoparticles.

II. METODS

This study examines the optical behavior of gold nanoparticles with various morphologies in both monomer and dimer states within the first biological window (650-950 nm). The morphologies of spheres, rods, cubes, and pyramids were all designed with equal volumes, including the dimers, to provide a comparative perspective on the effect of nanoparticle concentration in photothermal applications. The radius of the monomeric gold nanosphere was set at 20 nm, and the geometric specifications of the other nanoparticles, including the length and diameter of the nanorod, the side lengths of the cube, and the tetrahedral pyramid, were chosen to have a volume equal to that of the sphere. The aspect ratio of the nanorod was set to 3 to ensure that the LSPR wavelength of the nanorod falls within the first biological window [19]. Numerous studies have reported the synthesis of gold nanoparticles with these morphologies [20-26]. Figure 1 shows the nanoparticles studied in this research. As shown in the figure,

the distance between nanoparticles in the dimer structure was set to 1 nm to achieve the maximum field enhancement. Additionally, nanoparticles other than the nanosphere were arranged in two configurations to examine the effect of coupling (Figure 1a, second and third rows)

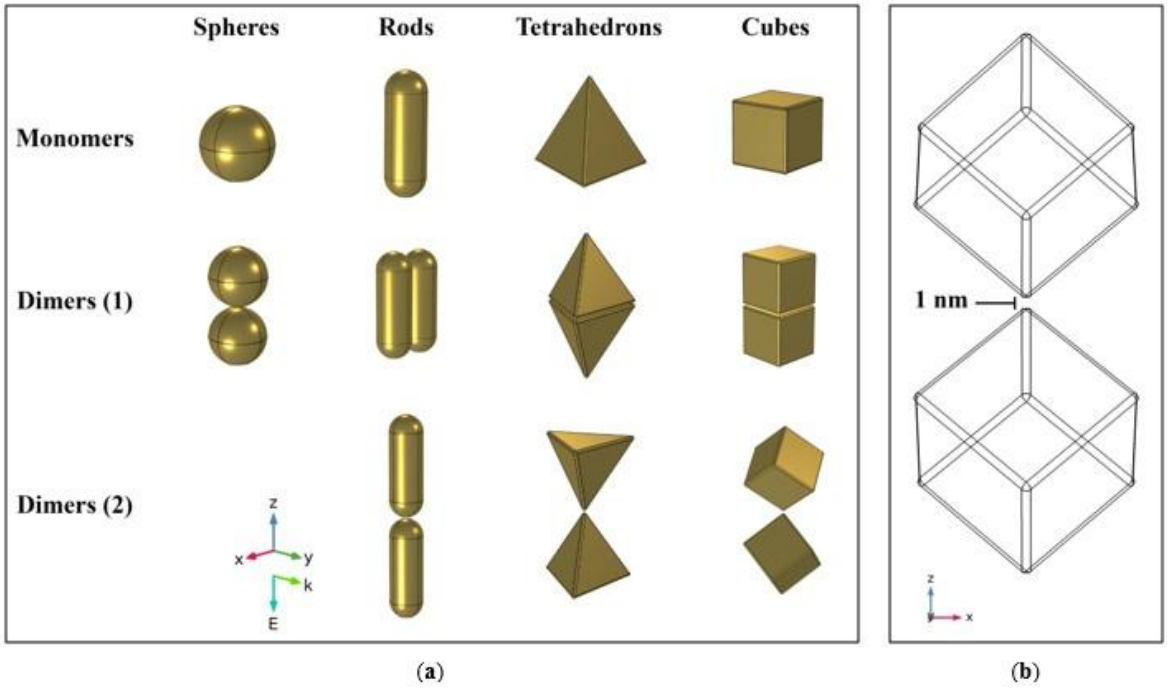

Fig **1. a**) Gold nanoparticles with morphologies of sphere, rod, pyramid, and cube in two structures: monomer (first row) and dimer (second and third rows), **b**) The arrangement of gold Nanocubes in the "dimers (2)" structure with a distance of 1 nm.

A numerical framework employing the Finite Element Method (FEM), known as COMSOL Multiphysics [27, 28], was used to solve the wave equation within the frequency domain of biological windows.

$$\nabla \times \left(\frac{1}{\mu_r}\nabla \times E_{sca}\right) - k_0^2\left(\varepsilon_r - j\frac{\sigma}{\omega\varepsilon_0}\right)E_{sca} = 0, \quad (1)$$

In equation (1), μ_r, ε_r, and σ represent the relative permeability, relative permittivity, and electrical conductivity of the materials, respectively. This equation provides the solution for the scattered field in terms of the local scattered electric field, E_{sca}. The total electric field, E, is the sum of the scattered electric field, E_{sca}, and the incident electric field, E_{inc}, around the nanoparticles. A spherical computational domain of water was created with the nanoparticle at its center. To prevent reflections from the water boundary, a perfectly matched layer (PML) with a thickness of 200 nanometers was applied to the outer edge of the water domain.

The solution for the scattered field was utilized to determine the optical cross-sections. The absorption, and scattering cross-sections (σ_{abs}, and σ_{sca}) for a nanoparticle are defined by the following equations.

$$\sigma_{abs} = \frac{W_{abs}}{I}, \quad (2)$$

$$\sigma_{sca} = \frac{W_{sca}}{I}, \quad (3)$$

Here, W_{abs} and W_{sca} represent the energies absorbed and scattered per unit time by the

nanoparticle, respectively, while I indicates the intensity of the incident light.

$$I = \frac{1}{2} c\varepsilon |E_{inc}|^2, \quad (4)$$

Based on commonly referenced values in the literature [10], light intensity of 1 mW/μm^{-2} was selected. These values were applied uniformly to all samples to evaluate the performance of the nanostructures under identical conditions.

The numerical solutions are utilized to calculate the absorbed and scattered powers in equations (2) and (3) as shown in the following adjusted equations.

$$W_{abs} = \frac{1}{2} \iiint_V Re[(\sigma E + j\omega D).E^* + j\omega B.H^*]\, dV, \quad (5)$$

$$W_{sca} = \frac{1}{2} \oiint_S Re[E_{sca} \times E_{sca}^*] \,.ndS \quad (6)$$

In the equation, the symbols $*$ and D denote the complex conjugate and the electric displacement field, respectively. Equation (5) requires integration over the volume of the nanoparticle, while equation (6) involves a surface integral over a virtual boundary surrounding the nanoparticle. The calculations were performed using the built-in functions of COMSOL Multiphysics. The Drude model was applied to determine the standard dispersive permittivity of gold [29]. The refractive index of the surrounding medium, which was water in this case, was maintained at a constant value of 1.33.

III. Results & Discussion

A. *Absorption & Scattering Cross-sections*

The dimer structure of nanoparticles is designed so that the nanoparticles have the highest (dimer1) and lowest (dimer2) adjacent surface areas. Additionally, the volume of each dimer was equal to the volume of the corresponding monomer to compare the optical properties of coupled nanoparticles against single nanoparticles at the same concentration. Figure 2 shows the absorption and scattering cross-sections of monomer and dimer gold nanoparticles. As seen in the figure, the absorption cross-sections related to the nanorod morphology are the highest, while the lowest absorption cross-sections are for nanospheres. However, coupled gold nanospheres exhibit a larger absorption cross-section compared to monomeric nanospheres of the same volume. Additionally, this coupling results in a 142 nm shift in the LSPR peak wavelength.

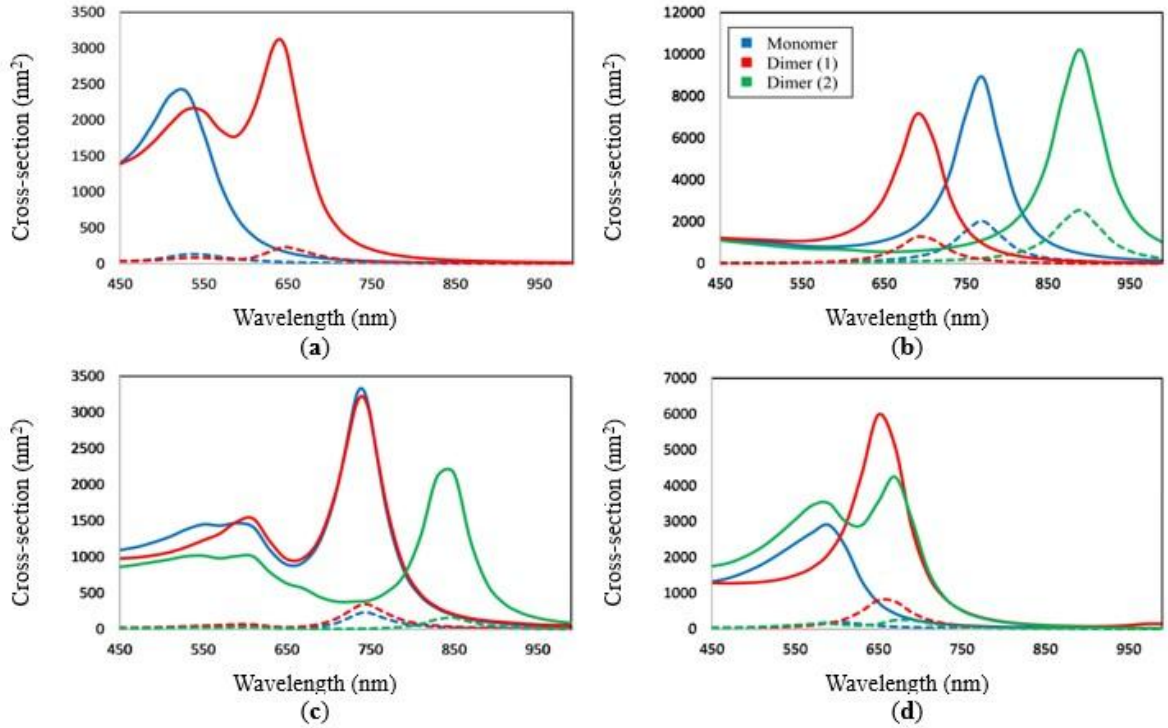

Fig **2.** Absorption and scattering cross-sections of monomer and dimer gold nanospheres (**a**), Nanorods (**b**), Nanopyramids (**c**), and Nanocubes (**d**). Solid lines and dashed lines indicate absorption cross-sections and scattering cross-sections, respectively.

In Figure 2b, it is notable that the side-by-side coupling of gold nanorods results in a lower LSPR than the same volume monomer and also reduces the LSPR peak wavelength. In contrast, end-to-end coupling of these nanoparticles increases the absorption and scattering cross-sections and the LSPR peak wavelength. It is observed that the difference in LSPR peak wavelength between the two coupled structures is about 200 nm. This difference will increase for Nanorods with Aspect Raito (AR) 4 and larger, such that the LSPR peak wavelength reaches the second biological window.

Considering the LSPR shifts in coupled nanorod structures and the specific laser wavelength for photothermal applications, maximum absorption by these nanoparticles may not occur, significantly reducing their efficiency.

The results of coupling nanopyramids are shown in Figure 2c. According to the figure, when coupled side-by-side, these gold nanoparticles exhibit optical behavior similar to that of a monomer nanoparticle of the same volume, such that there is no significant shift in the LSPR peak wavelength, nor a noticeable increase or decrease in the absorption cross-section. On the other hand, end-to-end coupling decreases the absorption cross-section but with an increase in the LSPR peak wavelength. The difference in LSPR peak wavelength between the two coupled structures in these nanoparticles is about 100 nm. This means that coupling nanopyramids is more controllable than coupling gold Nanorods and the LSPR of nanopyramids can be better tuned to the desired laser wavelength.

Coupling Nanocubes also increases the absorption cross-section (Figure 2d). As shown in the figure, side-by-side and end-to-end coupling of Nanocubes enhances the absorption cross-section by approximately 2 and 1.5 times, respectively, with the LSPR peak wavelength changes being around 10 nm, the smallest change among the nanoparticles studied in this

work. However, the notable point is the LSPR range of these nanostructures, which is at the beginning of the first biological window. Given the LSPR peak wavelength of the monomer Nanocube, which is outside the first biological window range (590 nm), a dispersion of these Nanocubes may not show maximum absorption, making them unsuitable for photothermal applications. Nevertheless, Nanocubes have a larger cross-section compared to nanopyramids.

One of the other parameters for comparing the optical behavior of nanoparticles is the PCE value. This value is obtained by dividing the absorption cross-section of nanoparticles by the sum of their absorption and scattering cross-sections ($\sigma_{abs}/\sigma_{abs}+\sigma_{sca}$) [30]. Table 1 presents the results obtained from the simulations of this study for a better comparison of the optical properties of nanoparticles. As it is clear, dimer (2) gold Nanocubes have a higher PCE compared to other nanoparticles. In contrast, although gold nanorods have a larger absorption cross-section, they have a lower PCE.

TABLE1. OPTICAL PROPERTIES OF MONOMER AND DIMER GOLD NANOPARTICLES

Morphology	Monomer			Dimer (1)			Dimer (2)		
	LSPR peak wavelength (nm)	σ_{abs} (nm^2)	PCE (%)	LSPR peak wavelength (nm)	σ_{abs} (nm^2)	PCE (%)	LSPR peak wavelength (nm)	σ_{abs} (nm^2)	PCE (%)
Sphere	530	2386	94.8	642	3118.4	93.3	-	-	-
Rod	765	9013.4	81.3	694	7257.4	84.6	886	10301	79.9
Pyramid	739	3336.5	93.6	740	3213.7	90.2	841	2133.6	93.6
Cube	590	2894.4	94.3	654	6054.2	88	664	4302.8	95.1

Figure 3 illustrates the comparison of the LSPR peak wavelength and the absorption cross-section of gold Nanorod, Nanopyramid, and Nanocube dimers. According to this figure, as mentioned, the widest range of LSPR peak wavelength variations pertains to nanorod dimers. In contrast, the narrowest range of this wavelength variation is observed in Nanocube dimers, although the wavelengths related to these nanoparticles fall at the beginning of the biological window. This comparison can provide insight into how significant variations in the LSPR peak wavelength due to nanoparticle coupling can lead to the overall LSPR peak wavelength of all nanoparticles in a system deviating from the selected laser wavelength. Ultimately, this can reduce the system's efficiency in absorbing light and converting it into heat.

Figure 3 also shows the range of absorption cross-section variations of coupled nanoparticles. It is observed that the highest and lowest absorption cross-sections, as well as the widest and narrowest ranges of absorption cross-section variations, correspond to coupled Nanorods and Nanopyramids, respectively.

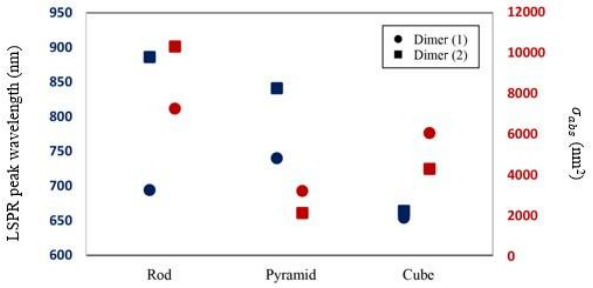

Fig **3.** Variation ranges of LSPR peak wavelength and absorption cross-section of coupled gold nanoparticles.

The variation ranges of LSPR peak wavelengths (indicated by blue symbols) and absorption cross-sections (shown by red symbols) for coupled gold nanoparticles are discussed. Dimeric Nanospheres display the most significant variation in LSPR peak wavelength, approximately 200 nm. In contrast, the coupling method for Nano-cubes shows little impact on their LSPR peak wavelength. Additionally, the changes in the absorption

cross-section of dimeric Nanorods are more pronounced compared to those of other Nano-dimers. This suggests that the optical properties of rod-shaped gold nanoparticles are especially sensitive to the chosen coupling method.

B. *Localized Field Enhancement*

Another important feature in comparing the performance of plasmonic nanoparticles in photothermal applications is their ability to enhance the local field near them. This field enhancement can be utilized in applications such as imaging, Surface-Enhanced Raman Spectroscopy (SERS), biosensors, nonlinear optics, and controlled drug delivery. Figure 4 shows the improvement of the local field at the LSPR peak wavelength of the nanostructures studied in this work. As observed, side-by-side coupling results in a slight reduction in the field around the nanoparticles. In contrast, end-to-end coupling significantly enhances the field in the gap between the nanoparticles by several folds. This enhancement reaches over 30 times for gold nanospheres, about 15 times for nanorods, over 1.5 times for nanopyramids, and over 5 times for Nano-cubes. This comparison is more evident in Figure 5. According to the figure, gold nanopyramids, whether in monomer or dimer structures, improve the field around them more than other nanoparticles.

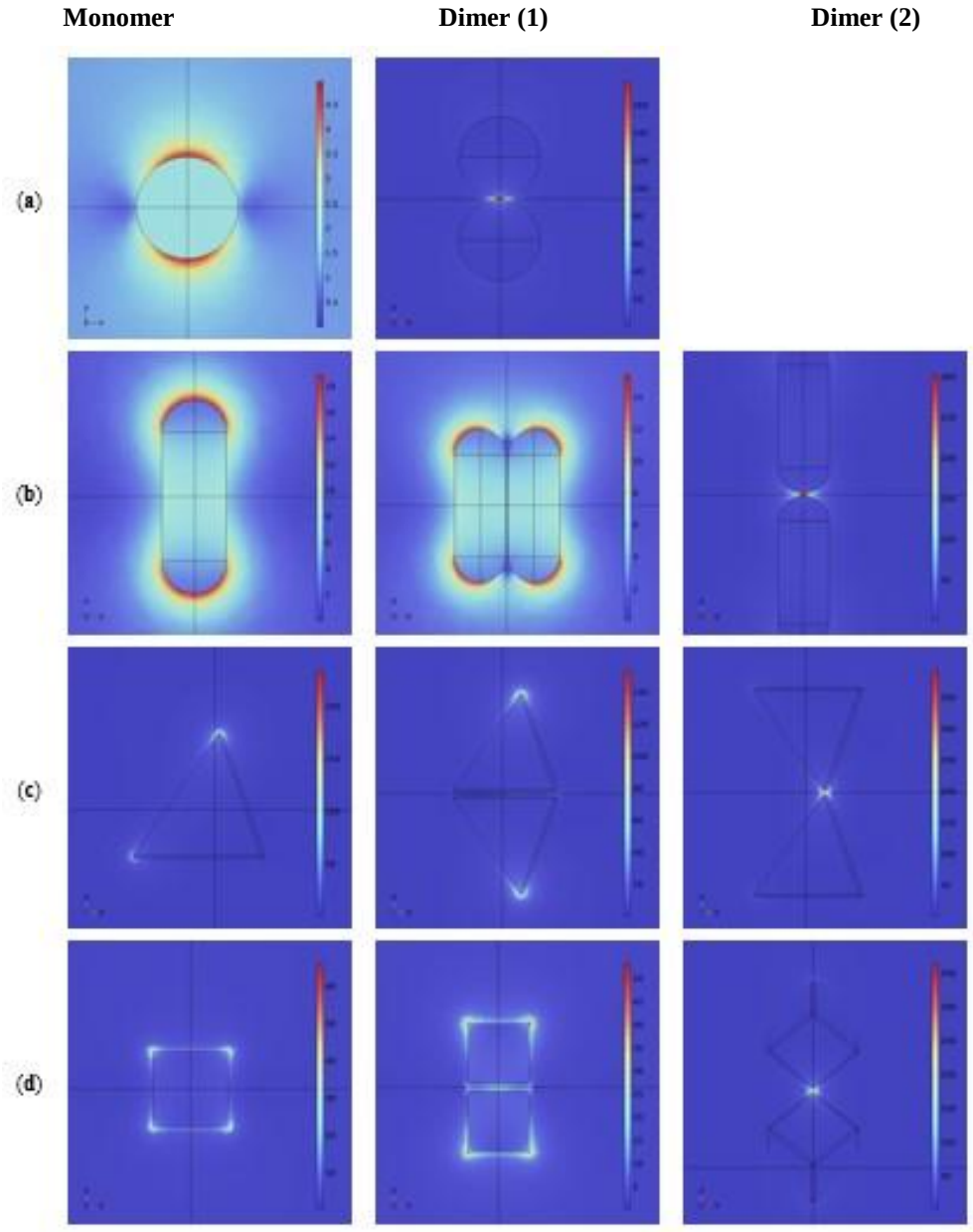

Fig **4.** Local field enhancement at the LSPR peak wavelength for gold Nanospheres (**a**), Nano-rods (**b**), Nano-pyramids (**c**) and Nano-cubes (**d**) in monomer and dimer configurations

(Note: all legends indicate the value of $|E/E_0|$.)

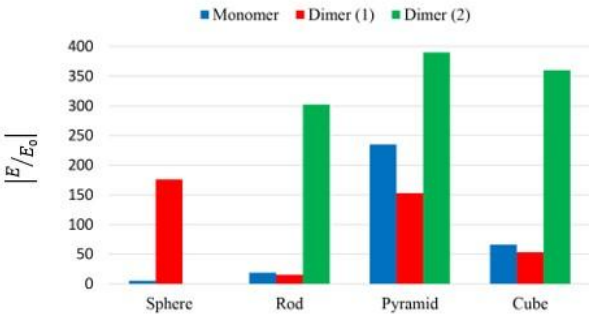

Fig **5.** Comparison of local field enhancement in gold monomer and dimeric nanostructures.

IV. Conclusion

In this study, we numerically investigated the optical behavior of gold nanoparticles with spherical, rod, pyramid (tetrahedral), and cubic morphologies in both monomer and dimer configurations for photothermal applications. The total volume of the dimer nanoparticles was kept equal to that of the monomer nanoparticles to provide insight into the effect of their concentration. Gold nanospheres, both as monomers and dimers, exhibited high PCE, but their LSPR peak wavelengths did not reach the first biological window. Gold nanorods, both as monomers and dimers, had the highest absorption cross-section but the lowest PCE. The LSPR peak wavelengths of coupled nanorods in side-by-side and end-to-end configurations were significantly different, making tuning the LSPR of these nanoparticles to the laser wavelength challenging. Gold nanopyramids showed the highest local field enhancement. Gold Nano-cubes also had high PCE values. When coupled, these nanoparticles had very close LSPR peak wavelengths, indicating that they can be tuned to the desired laser wavelength in either configuration. However, the LSPR peak wavelength of gold Nano-cube dimers was at the beginning of the first biological window, which could be a challenge for photothermal applications. Based on the results, gold tetrahedral nanopyramids can be considered the best candidates for photothermal applications due to their suitable PCE and their LSPR being in the first biological window. Additionally, there is a moderate difference in the LSPR peak wavelengths of these nanoparticles in side-by-side and end-to-end configurations. They also experience the highest field enhancement, especially in the end-to-end configuration.

Considering that the use of smaller nanoparticles increases the chance of their coupling, it can be said that these coupled nanoparticles exhibit significant optical properties compared to their monomer counterparts of the same volume. This includes the enhancement of the local field by dimer nanoparticles, which is several times greater than that of monomer nanoparticles. Additionally, the heat generated by these nanostructures can be calculated for further investigation.

References

[1] Zhao L. Zhang X. Wang X. Guan X. Zhang W. and Ma J. "Recent advances in selective photothermal therapy of tumor," Journal of Nanobiotechnology, vol. 19, pp. 1-15, 2021.

[2] Zhang L. Oudeng G. Wen F. and Liao G. "Recent advances in near-infrared-II hollow nanoplatforms for photothermal-based cancer treatment," Biomaterials Research, vol. 26, pp. 61, 2022.

[3] Yu S. Xia G. Yang N. Yuan L. Li J. Wang Q. Li D. Ding L. Fan Z. and Li J. "Noble Metal Nanoparticle-Based Photothermal Therapy: Development and Application in Effective Cancer Therapy," International Journal of Molecular Sciences, vol. 25, pp. 5632, 2024.

[4] Dykman L. and Khlebtsov N. "Gold nanoparticles in biomedical applications: recent advances and perspectives," Chemical Society Reviews, vol. 41, pp. 2256-2282, 2012.

[5] Amendola V. Pilot R. Frasconi M. Maragò O. M. Iatì, and M. A. "Surface plasmon resonance in gold nanoparticles: a review," Journal of Physics: Condensed matter, vol. 29, pp. 203002, 2017.

[6] Lv Z. He S. Wang Y. and Zhu X. "Noble metal nanomaterials for NIR- triggered photothermal therapy in cancer," Advanced Healthcare Materials, vol. 10, pp. 2001806, 2021.

[7] Breitenborn H. Dong J. Piccoli R. Bruhacs A. Besteiro L. Skripka A. Wang Z. Govorov A. Razzari L. and Vetrone F. "Quantifying the photothermal conversion efficiency of plasmonic nanoparticles by means of terahertz radiation," Apl Photonics, vol. 4, 2019.

[8] Smith A. M. Mancini M. C. and Nie S. "Second window for in vivo imaging," Nature Nanotechnology, vol. 4, pp. 710-711, 2009.

[9] Wu X. Suo Y. Shi H. Liu R. Wu F. Wang T. Ma L. Liu H. and Cheng Z. "Deep-tissue photothermal therapy using laser illumination at NIR-IIa window," Nano-Micro Letters, 12, pp.1-13, 2020.

[10] Baffou G. and Quidant R. "García de Abajo, F. J., Nanoscale control of optical heating in complex plasmonic systems," ACS nano, vol. 4, pp. 709-716, 2010.

[11] Farooq S. Rativa D. and de Araujo R. E. "Quantitative analysis of high performance plasmonic metamolecules for targeted deep tissues applications," Plasmonics, vol. 18, pp. 2475-2482, 2023.

[12] Sahu A. K. and Raj S. "Understanding the Coupling Mechanism of Gold Nanostructures by Finite-Difference Time-Domain Method," International Journal of Nanoscience 2022, vol. 21, pp. 2250007, 2023.

[13] Pratap D. Shah R. K. Khandekar S. and Soni S. "Photothermal effects in small gold nanorod aggregates for therapeutic applications," Applied Nanoscience, vol. 12, pp. 2045-2058, 2022.

[14] Sahu A. K. and Raj S. "Effect of plasmonic coupling in different assembly of gold nanorods studied by FDTD," Gold Bulletin, vol. 55, pp. 19-29, 2022.

[15] Pal S. K. Chatterjee H. and Ghosh S. K., "Manipulating the confinement of electromagnetic field in size-specific gold nanoparticles dimers and trimers," RSC advances, vol. 9, pp. 42145-42154, 2019.

[16] Khoury C. G. Norton S. J. and Vo-Dinh T. "Plasmonics of 3-D nanoshell dimers using multipole expansion and finite element method," Acs Nano, vol. 3, pp. 2776-2788, 2009.

[17] Lipchus E. J. FEM Simulations of Plasmon Field Enhancement in Gold Nanoparticle Dimers and Gold Nanoparticle-Nanorod Dimers, University of Massachusetts Boston, 2023.

[18] Mencarelli E. Fanò L. Tarpani L. and Latterini L. "Modelling the optical properties of metal nanoparticles: analytical vs finite elements simulation," Materials Today: Proceedings, vol. 2, pp. 161-170, 2015.

[19] Rajabpour V. Abbasian K. and Ertugrul M. "Core-Shell Plasmonic Nanostructures for Hyperthermia of Cancer and Tumor Cells," Plasmonics, pp. 1-13, 2024.

[20] Sun M. Cheng Z. Chen W. and Jones M. "Understanding symmetry breaking at the single-particle level via the growth of tetrahedron-shaped nanocrystals from higher-symmetry precursors," ACS nano, vol. 15, pp. 15953-15961, 2021.

[21] Pérez-Juste J. Pastoriza-Santos I. Liz-Marzán L. M. and Mulvaney P. "Gold nanorods: synthesis, characterization and applications," Coordination chemistry reviews, vol. 249, pp. 1870-1901, 2005.

[22] Wang Y. Chen J. Zhong Y. Jeong S. Li R. and Ye X. "Structural diversity in dimension-controlled assemblies of tetrahedral gold nanocrystals," Journal of the American Chemical Society, vol. 144, pp.13538-13546, 2022.

[23] Yoo S. Youn G. Lee H. Kwon J. S. Lee Y. and Lee S. "Synthesis of ultra- small gold nanorods: Effect of reducing agent on reaction rate control," Bulletin of the Korean Chemical Society, vol. 44, pp. 648-652, 2023.

[24] Huang C.-J. Wang Y.-H. Chiu P.-H. Shih M.-C. and Meen T.-H. "Electrochemical synthesis of gold nanocubes," Materials Letters, vol. 60, pp. 1896-1900, 2006.

[25] Khan A. W. Lali N. S. Sabei F. Y. Irfan M. I. Naeem-ul-Hassan M. Sher M. Safhi A. Y. Alsalhi A. Albariqi A. H. ans Kamli F.

"Sunlight-assisted green synthesis of gold nanocubes using horsetail leaf extract: A highly selective colorimetric sensor for Pb2+, photocatalytic and antimicrobial agent," Journal of Environmental Chemical Engineering, vol. 12, pp. 112576, 2024.

[26] Schwartzberg A. M. Olson T. Y. Talley C. E. and Zhang J. Z. "Synthesis characterization, and tunable optical properties of hollow gold nanospheres," The Journal of Physical Chemistry B, vol. 110, pp. 19935-19944, 2006.

[27] Multiphysics C. *Introduction to comsol multiphysics*®. COMSOL Multiphysics, Burlington, MA, accessed 1998**.**

[28] Pryor, R. W., Multiphysics modeling using COMSOL®: a first principles approach. Jones & Bartlett Publishers: 2009.

[29] Johnson P. B. and Christy R.-W. "Optical constants of the noble metals," Physical Review B, vol 6, pp. 4370, 1972.

[30] Liu, Y. Kangas J. Wang Y. Khosla K. Pasek-Allen J. Saunders A. Oldenburg S. and Bischof J. "Photothermal conversion of gold nanoparticles for uniform pulsed laser warming of vitrified biomaterials," Nanoscale, vol. 12, pp. 12346-12356, 2020.